Supplementary materials for:

Seeding Ductile Nanophase in Ceramic Grains

Chong Zhao [a, #], Hao Lu [a, #, *], Haibin Wang [a], Xuemei Liu [a], Zhigang Zak Fang [b, *], Chao Hou [a], and Xiaoyan Song [a, *]

[a] *College of Materials Science and Engineering, Key Laboratory of Advanced Functional Materials, Ministry of Education of China, Beijing University of Technology, Beijing 100124, P. R. China*

[b] *Department of Metallurgical Engineering, University of Utah, Salt Lake City, UT 84112, USA*

Co-first authors, *Correspondence: haolu@bjut.edu.cn (H. Lu), zak.fang@utah.edu (Z. Fang), and xysong@bjut.edu.cn (X. Song)

- **Composition analysis for the in-grain nanophase**
- **Evolution of the in-grain nanophase/WC interface**
- **Calculations regarding the formation of the in-grain nanophase**
- **Properties of samples for macroscopic mechanical tests**

1. Composition analysis for the in-grain nanophase

The image of the needle tip of the WC-10Co-0.8TaC sample for composition analysis by APT is shown in Figure 1(e). Table S1 gives the concentrations of W, C, and Co elements in different regions of the needle tip sample for APT measurements. It is found that the nanoparticles in the WC phase contain Co element mainly with a low concentration of W and C. Further, it shows that the atomic ratio of Co:W:C in the nanoparticle is 3:1:1 approximately, suggesting a solid solution of Co oversaturated with W and C. Namely, the nanoparticles are Co-rich nanophase.

Table S1. Concentrations of W, C, and Co elements in different regions of the needle tip in the APT measurements.

Element	W	C	Co
Needle (at.%)	50.10	49.49	0.10
Nanophase (at.%)	16.67	20.60	61.34
Interface (at.%)	54.68	39.75	4.37

With the increase of the TaC content, the size of the in-grain nanophase increases. The EDS mappings in Figure 2(k) confirm the Co-rich composition of the nanophase. It is measured that the concentrations of W and C decrease in the larger nanophase of the WC-10Co-1.5TaC sample, compared with those of the WC-10Co-0.8TaC sample, as shown in Table S2. This indicates that with the increase of TaC content, the Co proportion in the in-grain nanophase increases.

Table S2. W, Co, and C concentrations of in-grain nanophase with different sizes in samples with different TaC contents.

Samples	Particle size (nm)	W (at.%)	Co (at.%)	C (at.%)
WC-10Co-1.5TaC	105.89	6.05	90.44	3.51
	77.29	22.52	72.14	5.34
	65.81	16.96	80.79	2.25
	58.08	23.95	71.09	4.96
	38.06	26.35	65.70	7.95
WC-10Co-0.8TaC	8.30	16.67	61.34	20.60

2. Evolution of the in-grain nanophase/WC interface

With the increase in the size of the in-grain nanophase, its shape becomes irregular, and some of the large nanoparticles may have twisty boundaries, as shown in Figure S1. With this kind of morphology, the initial coherent or semi-coherent interfaces between the in-grain nanophase and WC matrix will become incoherent interfaces, as indicated in Figure S1(b) and (c).

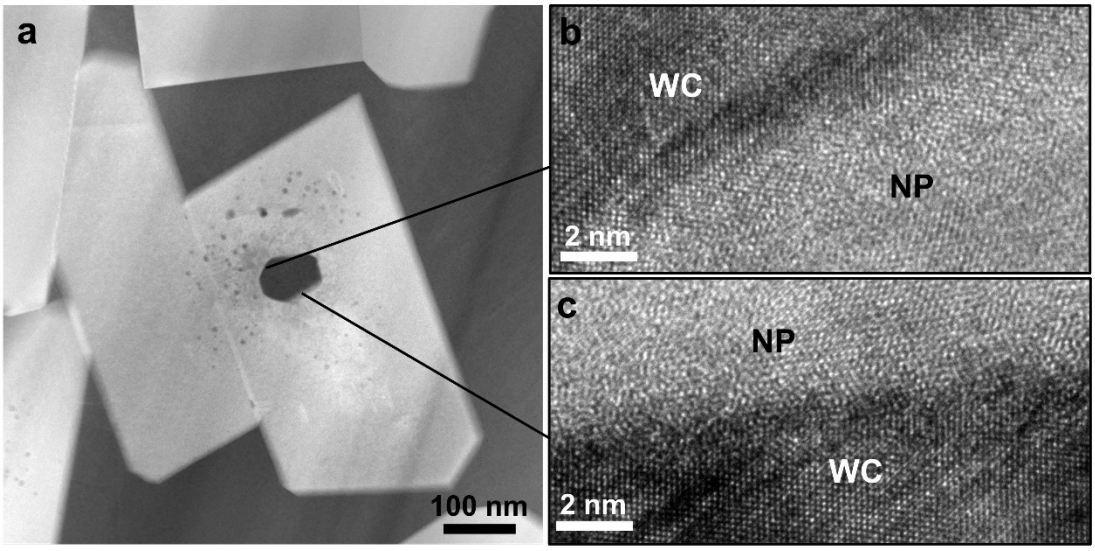

Figure S1. Interfaces between the large Co-rich nanophase and WC matrix. (a)

Microstructure image of the WC-10Co-1.5TaC sample with a large Co-rich in-grain nanophase. **(b, c)** HRTEM analysis of in-grain nanophase/WC interfaces.

3. Calculations related with the formation of the in-grain nanophase

From the experimental measurements in Figure 3(a) and (b), the concentration of Ta is obviously higher in the regions close to the edges of WC than in the center of WC. This result is well interpreted by the first-principles calculations. Figure S2 gives the models for calculations, where various occupations of Ta atoms are set up. It shows that the WC/Co interface with the C-terminated WC surface is the most stable. Then the calculations show that the segregation of Ta to the WC/Co interface can reduce both the formation energy and interface energy while increase the work of separation. These are all favorable to stabilize the structure and increase the interfacial strength.

The effect of carbon content on the formation of Co-rich in-grain nanophase is studied by calculations. Figure S3 gives the constructed models with carbon deficiency at different sites. It is found that the C-deficient site 3 at the interface is the most favorable in reducing the formation energy.

The locations for analysis of charge distributions presented in Figure 3(k) are shown in Figure S4. The calculations indicate that the deficiency of carbon atoms results in lattice distortion at the in-grain nanophase/WC interface, which increases the charge density between Co and C atoms at the interface (Figure 3k). Moreover, the formation energy of the nanophase in the WC grain decreases with the increase in the deficiency number of carbon atoms in the lattice structure.

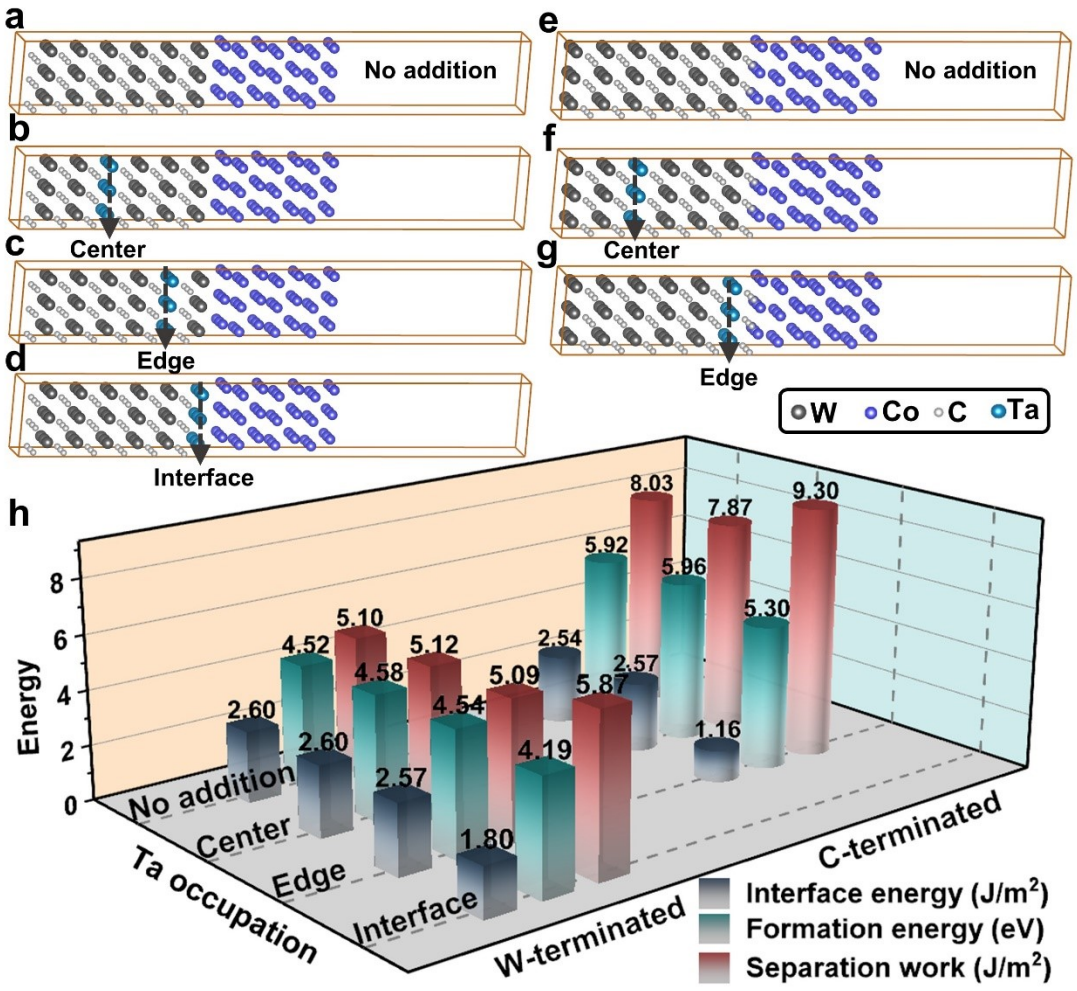

Figure S2. Calculations for the distribution characteristics of Ta atoms. (a-g) The computation models with Ta occupation sites in the WC interior, at the edge of WC, and at the WC/Co interface, where (a-d) for WC/Co interfaces with W-terminated WC and (e-g) for WC/Co interfaces with C-terminated WC. **(h)** The calculated formation energy, interface energy, and work of separation corresponding to the various configurations.

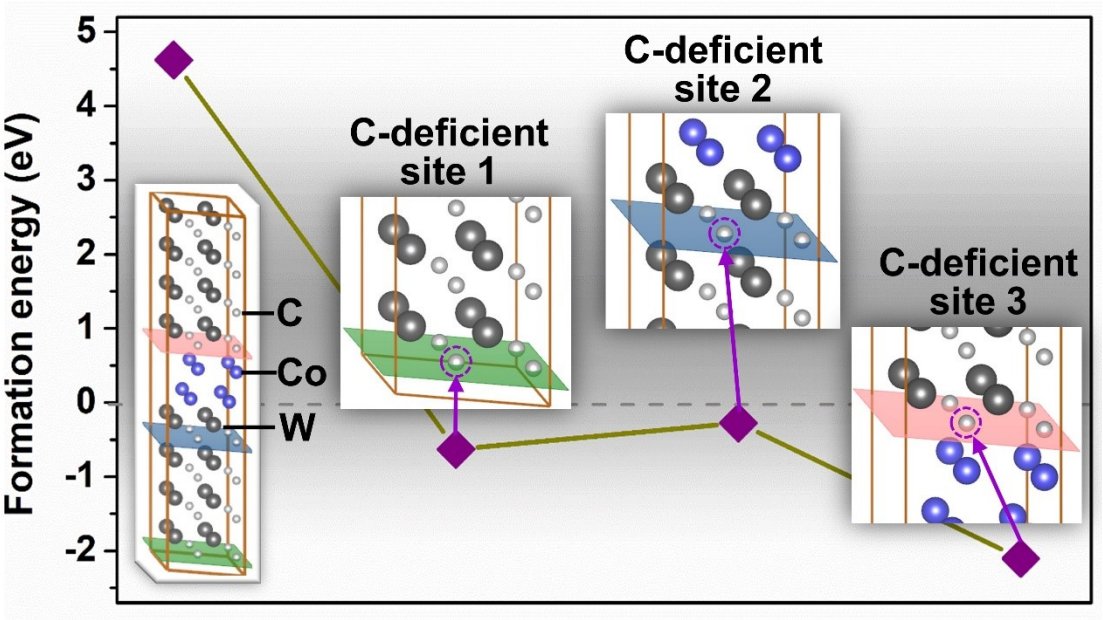

Figure S3. The computation models for the in-grain nanophase in WC with carbon deficiency at different sites, and the calculated formation energies corresponding to these structures. The crystallographical orientations at the WC/in-grain nanophase interface are $(0001)_{WC}$ // $(0001)_{NP}$ and $[1\bar{2}10]_{WC}$ // $[1\bar{2}10]_{NP}$, based on the microstructural analysis in Figure 2. The C-deficient sites: C deficient site 1 is inside the WC grain, C deficient site 2 is close to the in-grain nanophase/WC interface, and C deficient site 3 is at the in-grain nanophase/WC interface.

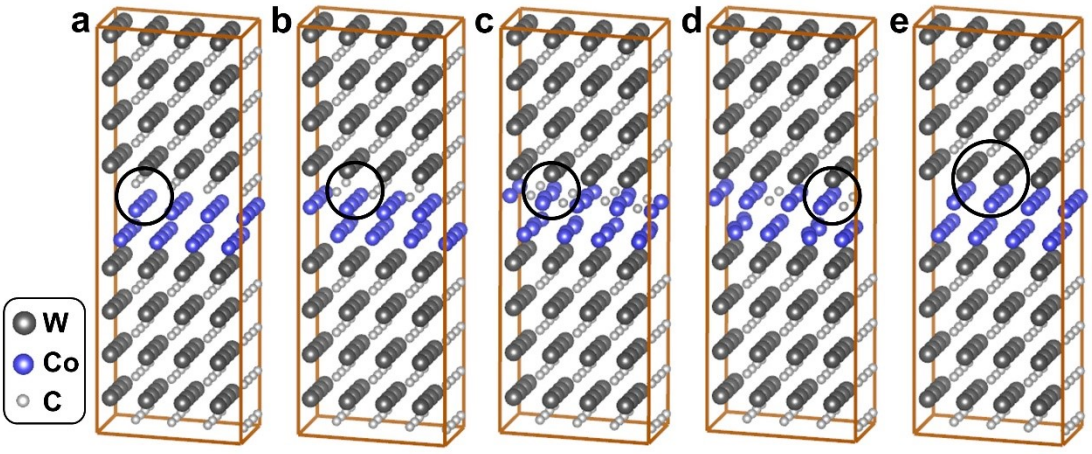

Figure S4. The computation models for the in-grain nanophase in WC after structural relaxation. (a) The nanophase in a WC grain with a precise stoichiometric ratio of W and C atoms. **(b-e)** The nanophase in WC grains with increased carbon

deficiency. The carbon deficient sites are taken at the WC/Co interface, because it is the most favorable to stabilize the structure, as indicated in Figure S3. The black circles in (a-e) indicate the locations for analysis of charge distributions in Figure 3(k).

4. Properties of samples for macroscopic mechanical tests

To distinguish the effect of in-grain nanophase on the mechanical properties of the cemented carbide, the macro-mechanical tests were first conducted for the bulk samples. The samples containing in-grain nanophase distributing in the central regions of WC grains were prepared from the in-situ synthesized WC-Co composite powder mixed with nanoscale TaC particles. The samples without in-grain nanophase were prepared from the directly mixed WC and Co powders. The XRD patterns of the in-situ synthesized WC-Co composite powder and the directly mixed powders are shown in Figure S5. The in-situ synthesized WC-Co composite powder contains a small amount of C-deficient phase in addition to WC and Co, which is critical to the formation of the in-grain Co-rich nanophase. Conversely, the mixture of WC and Co powders only contains WC and Co phases without any C-deficient phases. After sintering, all samples prepared from in-situ synthesized composite powder or mixture powder do not contain impurity, as shown in Figure S6. All these samples were fully densified after sintering, and they had a similar mean grain size (400～500 nm) and a homogeneous grain structure, as the SEM images shown in Figure S7.

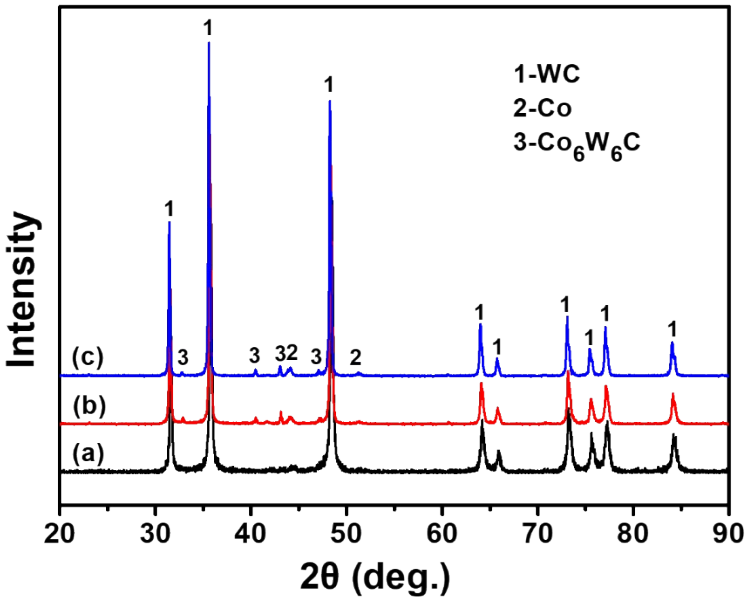

Figure S5. XRD patterns of the powders. (a) Mixture of WC and Co powders. **(b)** In-situ synthesized WC-Co composite powder. **(c)** Mixture of in-situ synthesized WC-Co composite and nanoscale TaC powders.

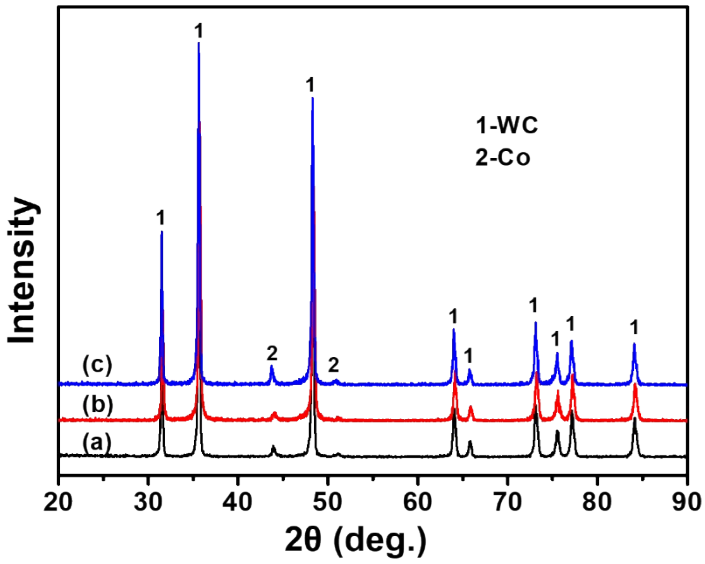

Figure S6. XRD patterns of the sintered cemented carbide samples prepared from different initial powders. (a) Mixture of WC and Co powders used as the sintering material. **(b)** In-situ synthesized WC-Co composite powder used as the sintering material. **(c)** Mixture of in-situ synthesized WC-Co composite and nanoscale TaC powders used as the sintering material.

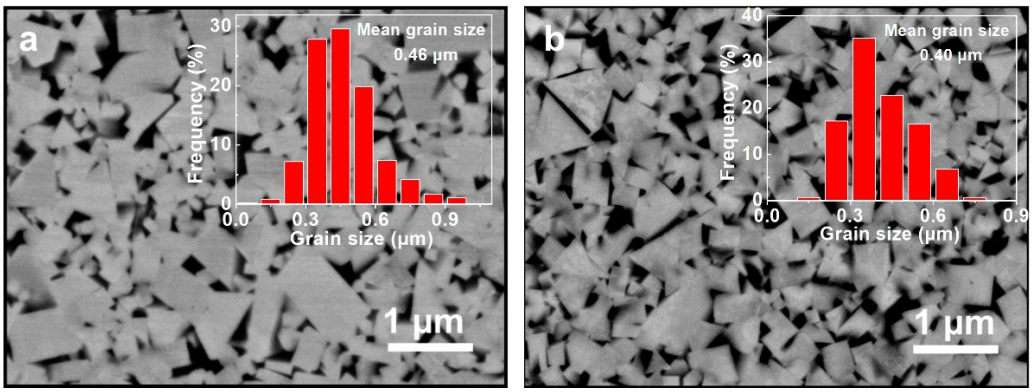

Figure S7. SEM images of the samples for macro-mechanical tests. (a) The WC-10Co-0.8TaC sample with in-grain nanophase distributing in the central regions of WC grains. **(b)** The WC-10Co sample without in-grain nanophase, prepared from the directly mixed WC and Co powders.

The measured Vickers hardness and fracture toughness of the samples are shown in Figure S8 and compared with the related data reported in the literature. It can be seen that the sample with in-grain nanophase distributing in the central regions of WC grains has the highest fracture toughness (K_{IC} = 11.8 ± 0.3 MPa·m$^{1/2}$) among all the samples and a good combination with the hardness (HV_{30} =1696 ± 15 kgf/mm^2).

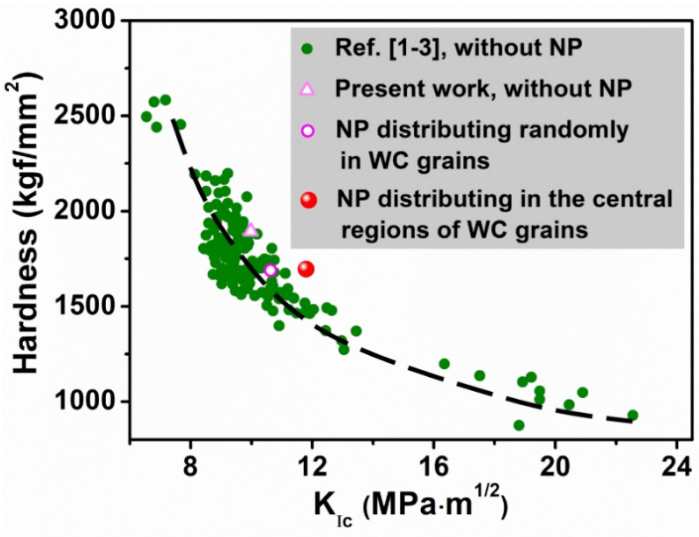

Figure S8. The measured Vickers hardness and fracture toughness of the samples

with and without in-grain nanophase and comparison with the data reported in the review articles [1-3].

[1] Farag, S., Konyashin, I. & Ries, B. The influence of grain growth inhibitors on the microstructure and properties of submicron, ultrafine and nano-structured hardmetals – a review. *Int. J. Refract. Met. Hard Mater.* **77**, 12–30 (2018).

[2] Aleksandrov F.T., Jakovljevic, S., Franz, M. & Jeren, I. Influence of grain growth inhibitors and powder size on the properties of ultrafine and nanostructured cemented carbides sintered in hydrogen, *Metals* **6**, 198 (2016).

[3] Schubert, W., Neumeister, H., Kinger, G. & Lux, B. Hardness to toughness relationship of fine-grained WC-Co hardmetals, *Int. J. Refract. Met. Hard Mater.* **16,** 133–142 (1998).

The micro-mechanical tests were conducted to reveal the local deformation and fracture characteristics of the different samples. Figure S9 and Figure S10 show the deformation and failure modes during uniaxial compression of the micropillar with and without in-grain nanophase respectively.

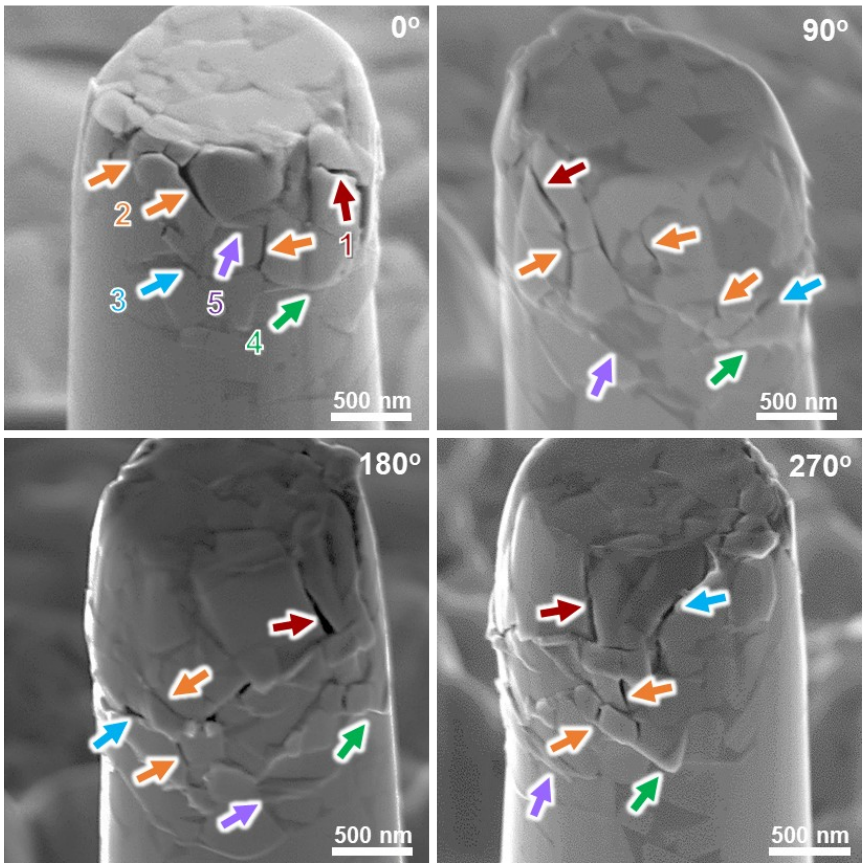

Figure S9. SEM micrographs showing the deformation and failure modes during

uniaxial compression of the micropillar with in-grain nanophase. (a-d) Viewed from 0°, 90°, 180°, and 270° directions, respectively. The arrows in different colors stand for failure modes of "1" - transgranular fracture, "2" - intergranular fracture, "3" - WC/Co interfacial fracture, "4" - WC grain gliding, and "5" - extrusion of Co binder.

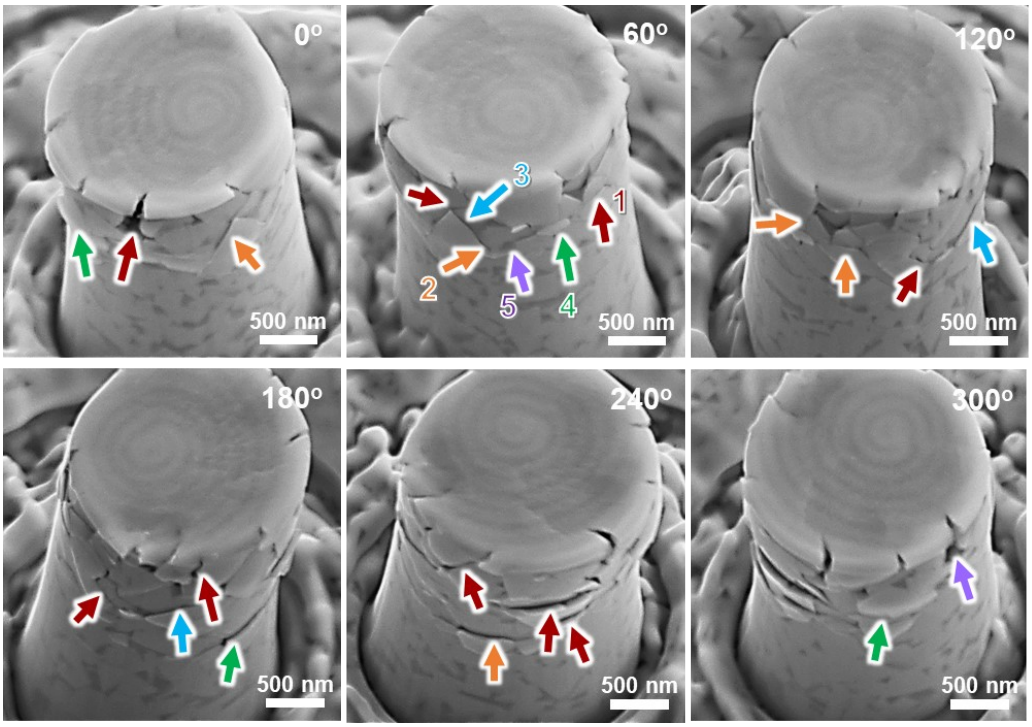

Figure S10. SEM micrographs showing the deformation and failure modes during uniaxial compression of the micropillar without in-grain nanophase. The arrows in different colors indicating: "1" - transgranular fracture, "2" - intergranular fracture, "3" - WC/Co interfacial fracture, "4" - WC grain gliding, and "5" - extrusion of Co binder.

In addition to the micropillar tests, experiments were conducted to investigate the cracks propagation paths in the samples after macro-mechanical tests. The main failure modes of WC-Co cemented carbides are intergranular and transgranular fractures. The lengths of these two kinds of cracks were counted at the corners of the Vickers hardness indentation on the samples. As shown in Figure S11, it is found that the transgranular

fracture is the dominant failure mode of the sample without in-grain nanophase. However, in the sample with in-grain nanophase, the length of transgranular cracks inside WC grains was reduced by more than 50% compared to that without in-grain nanophase. In this case, the intergranular fracture along the WC grain boundaries and WC/Co phase boundaries becomes the main failure mode in the sample with in-grain nanophase. This indicates that the ductile nanophase in WC grains plays a significant role in the mechanical behavior and failure mode of the cemented carbides.

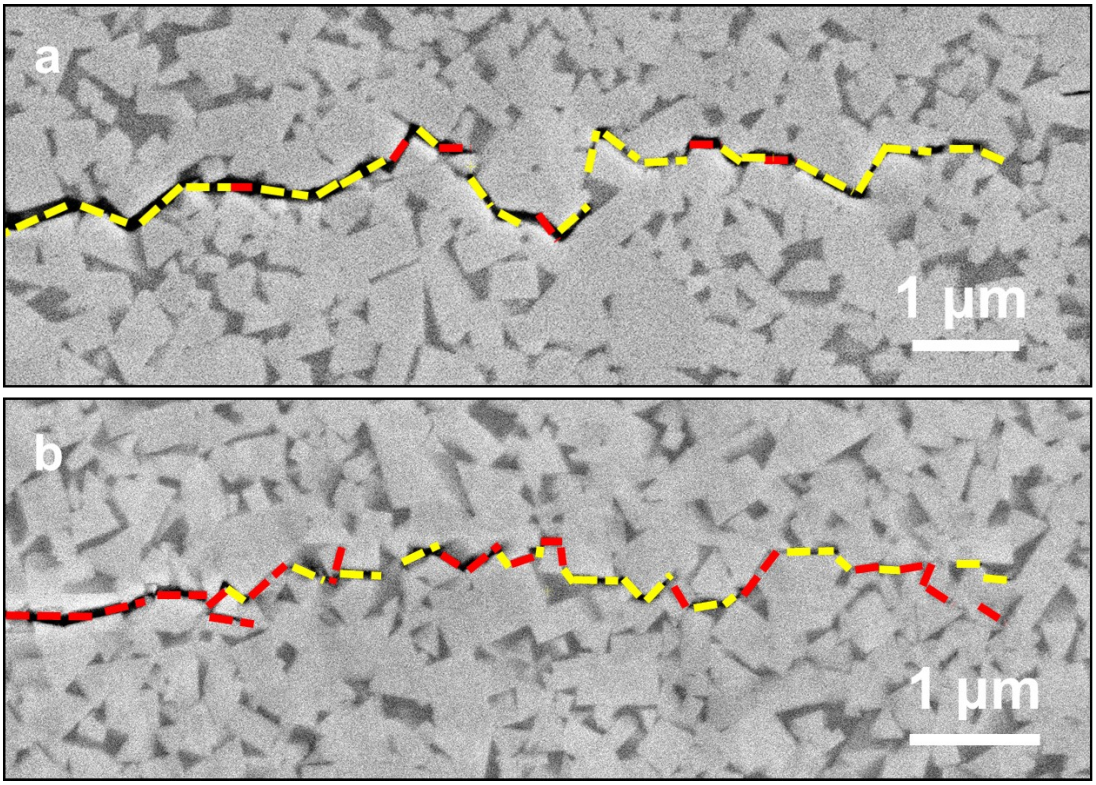

Figure S11. Crack propagation path of the samples after macro-mechanical tests. **(a)** The WC-10Co-0.8TaC sample with in-grain nanophase distributing in the central region of WC grains, and the transgranular cracks (red) have a ratio of 15%. **(b)** The WC-10Co sample without in-grain nanophase, prepared from the directly mixed WC and Co powders. The transgranular cracks (red) have a ratio of 58%.